AMERICAN SOCIETY FOR MICROBIOLOGY | Infection and Immunity®

BACTERIAL INFECTIONS

Malaria Parasite-Mediated Alteration of Macrophage Function and Increased Iron Availability Predispose to Disseminated Nontyphoidal *Salmonella* Infection

Kristen L. Lokken,[a] Annica R. Stull-Lane,[a] Kikkie Poels,[a] Renée M. Tsolis[a]

[a]Department of Microbiology & Immunology, School of Medicine, University of California at Davis, Davis, California, USA

ABSTRACT Disseminated infections with nontyphoidal *Salmonella* (NTS) are a significant cause of child mortality in sub-Saharan Africa. NTS infection in children is clinically associated with malaria, suggesting that malaria compromises the control of disseminated NTS infection. To study the mechanistic basis for increased NTS susceptibility, we utilized a model of concurrent infection with *Salmonella enterica* serotype Typhimurium and *Plasmodium yoelii nigeriensis* (*P. yoelii*). Underlying malaria blunted monocyte expression of Ly6C, a marker for inflammatory activation, and impaired recruitment of inflammatory cells to the liver. Hepatic mononuclear phagocytes expressed lower levels of inducible nitric oxide synthase, tumor necrosis factor alpha, and granulocyte-macrophage colony-stimulating factor and showed increased levels of production of interleukin-10 and heme oxygenase-1, indicating that the underlying malaria modifies the activation state and inflammatory response of mononuclear phagocytes to NTS. *P. yoelii* infection also increased intracellular iron levels in liver mononuclear cells, as evidenced by elevated levels of ferritin and by the rescue of an *S.* Typhimurium *tonB feoB* mutant defective for iron uptake. In addition, concurrent *P. yoelii* infection partially rescued the systemic colonization defect of an *S.* Typhimurium *spiB* mutant defective for type III secretion system 2 (T3SS-2), indicating that the ability of phagocytic cells to limit the spread of *S.* Typhimurium is impaired during concurrent *P. yoelii* infection. These results show that concurrent malaria increases susceptibility to disseminated NTS infection by blunting macrophage bactericidal mechanisms and providing an essential nutrient that enhances bacterial growth.

KEYWORDS *Salmonella*, coinfection, iron, macrophage, malaria

Nontyphoidal *Salmonella* (NTS) infections in immunocompetent individuals normally cause a localized, self-limiting gastroenteritis (1). In sub-Saharan Africa, NTS has become one of the most common causes of bloodstream infection in immunocompromised individuals, such as young children and HIV-infected adults (2). Epidemiological studies have identified malnutrition and severe malarial anemia to be risk factors for the development of systemic NTS infection in young children (3–5). In particular, these studies have demonstrated a strong association between disseminated NTS infection and *Plasmodium falciparum* malaria (2, 6); however, the mechanism by which malaria promotes increased susceptibility to systemic NTS infection is incompletely understood.

The etiology of severe malarial anemia encompasses a variety of factors that include hemolysis of infected and uninfected red blood cells (RBCs) and erythrophagocytosis by macrophages (7). Phagocytes, such as macrophages, are responsible for the clearance of circulating heme produced from the lysis of red blood cells. In order to detoxify the accumulating heme, phagocytes upregulate the enzyme heme oxygenase-1, which

Received 19 April 2018 **Returned for modification** 7 May 2018 **Accepted** 28 June 2018

Accepted manuscript posted online 9 July 2018

Citation Lokken KL, Stull-Lane AR, Poels K, Tsolis RM. 2018. Malaria parasite-mediated alteration of macrophage function and increased iron availability predispose to disseminated nontyphoidal *Salmonella* infection. Infect Immun 86:e00301-18. https://doi.org/10.1128/IAI.00301-18.

Editor Manuela Raffatellu, University of California San Diego School of Medicine

Address correspondence to Renée M. Tsolis, rmtsolis@ucdavis.edu.

degrades heme to biliverdin, carbon monoxide, and iron (reviewed in reference 8). The iron liberated from heme is exported to the cytosol, where it is incorporated into ferritin molecules. Increased stores of iron-laden ferritin have been shown to enhance the survival of *Salmonella enterica* serotype Typhimurium in macrophages (9). Additionally, it was recently demonstrated that induction of hemolytic anemia during malaria impairs the neutrophil oxidative burst capacity via induction of heme oxygenase-1 (10). Consequently, the dampened neutrophil bactericidal response during malaria leads to an increase in the systemic growth of *S.* Typhimurium. Further, *in vitro* expression of heme oxygenase-1 in a murine macrophage cell line enhances the intracellular survival of *S.* Typhimurium and reduces the formation of reactive oxygen and nitrogen species and tumor necrosis factor alpha (TNF-α) production (11). This previous work suggests that underlying malaria may dampen the inflammatory responses of macrophages.

Our previous work showed that the parasite-mediated induction of both interleukin-10 (IL-10) and anemia increases susceptibility to NTS bacteremia during malaria (12). Within systemic tissue, we found that both phagocytic cell production and the response of phagocytic cells to IL-10 during underlying *Plasmodium yoelii nigeriensis* (*P. yoelii*) infection impairs bacterial clearance. IL-10 is known to polarize macrophages to an anti-inflammatory state. Additionally, exogenous IL-10 can inhibit a variety of macrophage functions, including the release of proinflammatory mediators, phagocytosis, and antigen presentation. Therefore, we sought to determine whether underlying *P. yoelii* infection enhances susceptibility to invasive NTS infection by modulating macrophage activation and bactericidal activity.

RESULTS

Enhanced systemic colonization with *S.* Typhimurium is independent of T3SS-2 during concurrent *P. yoelii* infection. In order to determine if phagocytic cells are unable to restrict the systemic growth of NTS during malaria, we used our previously published model of *P. yoelii* and *S.* Typhimurium coinfection in mice (12). As shown before, concurrent *P. yoelii* infection led to a significant increase in the liver bacterial burden (Fig. 1a). In order to persist systemically, *S.* Typhimurium relies on the expression of the type III secretion system 2 (T3SS-2), encoded on the *Salmonella* pathogenicity island 2 (SPI-2). T3SS-2 facilitates the translocation of effectors across the *Salmonella*-containing vacuole (SCV) to promote the integrity of the SCV as a specialized niche for bacterial replication. The loss of T3SS-2 reduces the ability of *S.* Typhimurium to spread from infected phagocytes at systemic sites (13). Considering that professional phagocytes, generally, macrophages, harbor the majority of *S.* Typhimurium bacteria during infection (14, 15), we infected mice with a T3SS-2-defective mutant (*S.* Typhimurium *spiB*) to determine the effect of malaria on systemic bacterial colonization. As expected, the *spiB* mutant was defective for colonization of the liver and spleen when administered by the oral route (Fig. 1b) or the intraperitoneal (i.p.) route (see Fig. S3 in the supplemental material). However, concurrent *P. yoelii* infection significantly increased the systemic colonization of the *S.* Typhimurium *spiB* mutant after oral (Fig. 1b) or i.p. (Fig. S2) inoculation, indicating that the ability of phagocytic cells to limit the spread of *S.* Typhimurium is impaired during concurrent *P. yoelii* infection.

Malaria parasite-induced IL-10 reduces inflammatory monocyte infiltration. Previously, we found that *P. yoelii* infection blunted expression of neutrophil chemokines via parasite-mediated induction of IL-10 (12). As a result, neutrophil recruitment to the liver in response to *S.* Typhimurium infection was significantly decreased. Since neutrophil extravasation precedes the influx of mononuclear phagocytes (14, 16), we questioned whether the underlying *P. yoelii* infection also blunted the recruitment of inflammatory monocytes. In order to test this idea, flow cytometry was employed to characterize the infiltrating inflammatory monocyte ($CD11b^+$ $Ly6G^-$ $Ly6C^+$) population (17, 18) in the liver. Similar to what was observed with neutrophils (12), we found a significant decrease in the percentage and number of inflammatory monocytes in the liver of coinfected mice compared to *S.* Typhimurium-infected mice (Fig. 1c and d; see

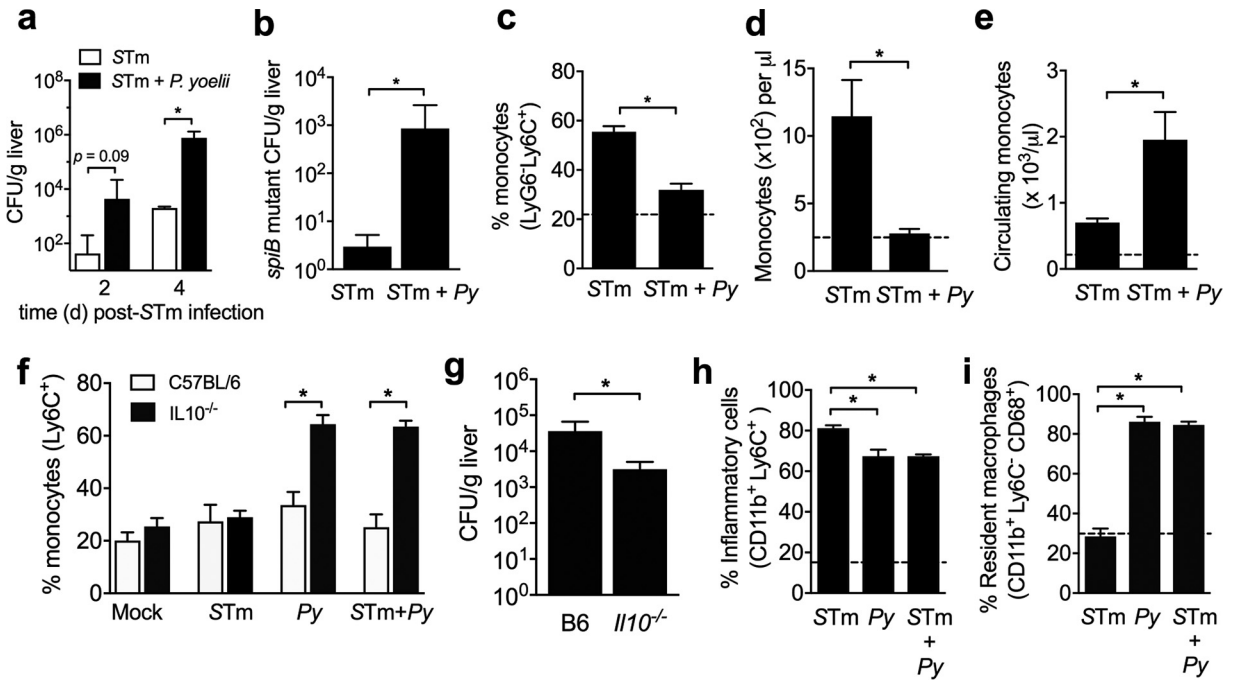

FIG 1 (a) Colonization (as the number of CFU) of the liver at 2 and 4 days after IG infection of *P. yoelii*-infected or uninfected CBA/J mice with *S.* Typhimurium ($n = 3$ or 4). Data are shown as the mean ± SEM. Statistical significance was determined using an unpaired Student *t* test on log-transformed values. *, $P < 0.05$. (b) Number of CFU in the liver at 5 days after IG infection of *P. yoelii*-infected or uninfected CBA/J mice with an SPI-2 T3SS *S.* Typhimurium mutant (*spiB*) ($n = 10$). Data are shown as the mean ± SEM and represent the results from two independent experiments. (c, d) Percentage (c) and number (d) of inflammatory monocytes (CD11b$^+$ Ly6G$^-$ Ly6C$^+$) in the liver from *S.* Typhimurium-infected and coinfected mice ($n = 4$ to 5). The number of inflammatory monocytes (singlet live CD3$^-$ B220$^-$ NK1.1$^-$ CD11b$^+$ Ly6G$^-$ Ly6C$^+$) per 4×10^6 liver cells was determined by the use of AccuCount beads. Data are shown as the mean ± SEM. The dotted line represents the average for two mock-infected controls. (e) Number of circulating monocytes (10^3 per microliter) determined by complete blood counts ($n = 4$ to 5). The dashed line represents the average for two mock-infected controls. Data are shown as the mean ± SEM. (f) Percentage of inflammatory monocytes (CD11b$^+$ Ly6G$^-$ Ly6C$^+$) in the liver from wild-type C57BL/6J *Slc11a1*$^{+/+}$ and C57BL/6J *Slc11a1*$^{+/+}$ *Il10*$^{-/-}$ mice infected with *P. yoelii* or *S.* Typhimurium, coinfected mice, or uninfected controls. Data are shown as the mean ± SEM and represent the results from two independent experiments ($n = 4$ to 7). (g) Number of CFU in the liver from wild-type C57BL/6J (B6) *Slc11a1*$^{+/+}$ and C57BL/6J *Slc11a1*$^{+/+}$ *Il10*$^{-/-}$ coinfected mice at 2 days postinfection with *S.* Typhimurium ($n = 4$ to 7). Data are shown as the mean ± SEM and represent the results from two independent experiments. (h) Percentage of inflammatory phagocytes (singlet live CD3$^-$ B220$^-$ Nk1.1$^-$ CD11b$^+$ Ly6C$^+$) in the liver from *S.* Typhimurium-infected, *P. yoelii*-infected, and coinfected mice ($n = 4$ to 9). (i) Percentage of liver macrophages (singlet live CD3$^-$ B220$^-$ Nk1.1$^-$ CD11b$^+$ Ly6C$^-$ CD68$^+$) from *S.* Typhimurium-infected, *P. yoelii*-infected, and coinfected mice ($n = 4$ to 9). Data are shown as the mean ± SEM. For panels b to i, statistical significance was determined using an unpaired Student *t* test on log-transformed or arc-sin-transformed values. *, $P <$ 0.05. *S*tm, *S.* Typhimurium; *Py*, *P. yoelii*. See also Fig. S1 in the supplemental material.

also Fig. S1 in the supplemental material). Conversely, the circulating numbers of monocytes were significantly increased in coinfected mice, indicating that bone marrow production of monocytes was not impacted during the underlying *P. yoelii* infection (Fig. 1e). The reduction of inflammatory monocyte numbers in the livers of mice coinfected with *S.* Typhimurium and *P. yoelii* was partially dependent on the production of IL-10, since the proportion of inflammatory monocytes in the liver was significantly increased in coinfected *Il10*$^{-/-}$ mice compared to coinfected IL-10-sufficient controls (Fig. 1f). As observed previously, a lack of IL-10 during coinfection significantly reduced the liver bacterial burden (Fig. 1g). Together, these results indicate that parasite-mediated IL-10 dampens inflammatory phagocyte recruitment and, consequently, increases susceptibility to systemic NTS infection.

Although the influx of inflammatory macrophages was reduced in response to *S.* Typhimurium infection during malaria, it was unclear how resident macrophage populations were affected. To address this question, an additional macrophage marker, CD68, was used to further characterize liver macrophages (19). As expected, the majority of CD11b$^+$ phagocytes in the liver after *S.* Typhimurium infection consisted of inflammatory cells (Ly6C$^+$), which were composed primarily of inflammatory monocytes (Ly6C$^+$ Ly6G$^-$) and neutrophils (Ly6C$^+$ Ly6G$^+$) (Fig. 1h). However, the underlying *P. yoelii* infection significantly dampened liver inflammatory phagocyte recruitment

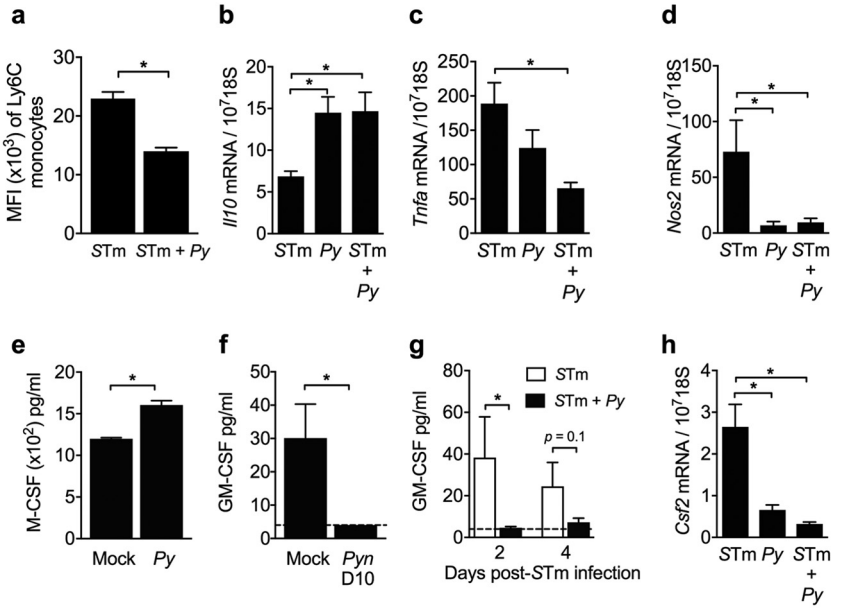

FIG 2 (a) Median fluorescent intensity (MFI) of surface Ly6C on liver monocytes in the CD11b$^+$ population from *S.* Typhimurium-infected and coinfected mice at 4 days after *S.* Typhimurium infection ($n = 4$ to 5). Data represent the mean ± SEM. CD11b$^+$ liver cells were enriched by positive selection from *S.* Typhimurium-infected, *P. yoelii*-infected, and coinfected CBA/J mice at 4 days after *S.* Typhimurium infection ($n = 3$ to 9). (b to d) Expression of IL-10 (*Il10*) (b), TNF-α (*Tnfa*) (c), and Nos2 (*Nos2*) (d) determined by quantitative RT-PCR. Data represent the mean ± SEM and are from two independent experiments. (e, f) Circulating levels of M-CSF (e) and GM-CSF (f) from mock-infected and *P. yoelii*-infected mice at day 10 (D10) after parasite infection ($n = 3$ to 4). Data represent the mean ± SEM. The dotted line represents the detection limit of 4 pg/ml. (g) Circulating GM-CSF concentrations in *S.* Typhimurium-infected and coinfected mice at 2 and 4 days after *S.* Typhimurium infection ($n = 3$ to 4). Data represent the mean ± SEM. The dashed line represents the detection limit of 4 pg/ml. (h) Expression of GM-CSF (*Csf2*) from CD11b$^+$ liver cells isolated from *S.* Typhimurium-infected, *P. yoelii*-infected, and coinfected mice 4 days after *S.* Typhimurium infection ($n = 3$ to 9). Data represent the mean ± SEM and are from two independent experiments. Statistical significance was determined using an unpaired Student *t* test on log-transformed values. *, $P < 0.05$. See also Fig. S2 in the supplemental material.

(Fig. 1h). Despite a reduction in the percentage of inflammatory phagocytes, both *P. yoelii*-infected and coinfected mice maintained higher numbers of resident liver macrophages (CD11b$^+$ Ly6C$^-$ CD68$^+$) than *S.* Typhimurium-infected mice (Fig. 1i). In the context of *S.* Typhimurium infection, it is possible that the expansion of macrophages enlarges the niche for bacterial replication. Therefore, in combination with a reduced influx of neutrophils and inflammatory monocytes, two phagocyte populations primed to kill *S.* Typhimurium, it is likely that alteration of the macrophage population during *P. yoelii* infection allows *S.* Typhimurium to increase its initial colonization.

Concurrent *P. yoelii* infection shifts the activation state of macrophages. In addition to the decreased infiltration of inflammatory monocytes during coinfection (Fig. 1c and d), we also observed a significant reduction in the surface expression of lymphocyte antigen 6 complex locus C1 (Ly6C) on monocytes from coinfected mice (Fig. 2a). Expression of Ly6C can be used to identify inflammatory monocytes (17, 18). It was observed that Ly6C^{high} monocytes are recruited to mucosal tissue during *S.* Typhimurium infection and that these cells express high levels of inducible nitric oxide synthase (iNOS) and TNF-α (20). Therefore, the reduced expression of Ly6C on monocytes during coinfection indicated that concurrent *P. yoelii* infection dampens both the recruitment and the activation of inflammatory monocytes in response to *S.* Typhimurium infection. To determine whether concurrent *P. yoelii* infection modulates activation of liver monocytes and macrophages, we isolated CD11b$^+$ cells from the livers of *S.* Typhimurium-infected, *P. yoelii*-infected, and coinfected mice. RNA analysis of CD11b$^+$ liver macrophages showed that expression of IL-10, an anti-inflammatory mediator, from *P. yoelii*-infected and coinfected mice was significantly increased com-

pared to that from *S*. Typhimurium-infected mice (Fig. 2b). In contrast, hepatic macrophage expression of inflammatory mediators, including *Tnfa* ($P = 0.0001$) and *Nos2* ($P < 0.0001$), was significantly reduced in coinfected mice compared to mice infected with *S*. Typhimurium alone (Fig. 2c and d). These results suggest that the underlying *P. yoelii* infection modulates the activation of macrophages by shifting their phenotype to an anti-inflammatory state.

In addition to IL-10, the colony-stimulating factors have been implicated in driving the polarization of macrophages during infection. Granulocyte-macrophage colony-stimulating factor (GM-CSF) and macrophage colony-stimulating factor (M-CSF) were first discovered by their abilities to generate *in vitro* colonies of mature myeloid cells from precursor cells in the bone marrow (21; reviewed in reference 22). Many studies have shown that GM-CSF drives bone marrow macrophages to a proinflammatory (M1) state, while M-CSF induces bone marrow macrophages to an anti-inflammatory (M2) state (23–25). It has been proposed that because of the high levels of M-CSF and the low levels of GM-CSF found under steady-state conditions (22), M-CSF drives the polarization of macrophages to an M2 state during homeostasis (24). Induction of GM-CSF by macrophages is increased after lipopolysaccharide stimulation *in vitro* (26, 27), and the loss of GM-CSF was shown to delay inflammation and impair resistance to *S. Typhimurium* infection in mice (28). During *P. yoelii* infection, the circulating levels of M-CSF increased during peak parasitemia (day 10) compared to those in the controls (Fig. 2e). In contrast, the levels of GM-CSF were below the limit of detection (4 pg/ml) in *P. yoelii*-infected mice, while the levels of GM-CSF in uninfected mice averaged 30 pg/ml (Fig. 2f). These results suggest that the underlying *P. yoelii* infection promotes the polarization of M2-like macrophages through inhibition of GM-CSF production. In order to mitigate the effects of M-CSF on the macrophage population, we treated coinfected mice with an anti-CSF1 (M-CSF) antibody or isotype control 1 day prior to and after *S*. Typhimurium infection (Fig. S2a). Blockade of M-CSF did not significantly impact the systemic bacterial burden in the liver or blood compared to that in mice treated with a control (Fig. S2b and c). Circulating M-CSF levels were similar between *S*. Typhimurium-infected and coinfected mice. However, there was a significant reduction in the levels of M-CSF in coinfected mice compared to *P. yoelii*-infected mice, which suggested that *S*. Typhimurium infection dampens the parasite-mediated induction of M-CSF (Fig. S2d). Although we were previously able to restore the control of systemic bacteria during coinfection by blockade of IL-10 (12), blockade of M-CSF alone was not sufficient to improve clearance. This finding raises the possibility that the increased M-CSF expression observed during *P. yoelii* infection acts in concert with IL-10 to impact macrophage bactericidal activity; however, in the absence of M-CSF, IL-10 is sufficient to shift the macrophage phenotype.

Although there were no differences in the levels of M-CSF between *S*. Typhimurium-infected and coinfected mice, the levels of GM-CSF were significantly reduced in coinfected mice compared to *S*. Typhimurium-infected mice 2 days after bacterial infection (Fig. 2g). Further, the expression of *Csf2* (encoding GM-CSF) by $CD11b^+$ liver macrophages was significantly blunted in *P. yoelii*-infected ($P = 0.04$) and coinfected mice ($P < 0.0001$) compared to mice infected only with *S*. Typhimurium (Fig. 2h). Taken together, these results suggest that a reduction of GM-CSF levels during coinfection contributes to the shift in the macrophage phenotype toward an anti-inflammatory state and, consequently, increases susceptibility to invasive NTS infection.

S. Typhimurium benefits from increased iron availability during concurrent *P. yoelii* infection. The clinical hallmark of malaria is hemolysis of red blood cells, which leads to severe anemia. Elevated levels of lactate dehydrogenase (LDH) in serum are associated with conditions causing intra- and extravascular hemolysis, such as hemolytic anemia. Measurement of serum LDH levels from *S*. Typhimurium-infected, *P. yoelii*-infected, and coinfected mice by enzyme-linked immunosorbent assay (ELISA) showed that the underlying *P. yoelii* infection significantly increased LDH levels, suggestive of hemolytic anemia (Fig. 3a; see also Fig. S3 in the supplemental material). As mentioned above, the induction of hemolytic anemia results in an increase in circulating heme levels. In order to prevent excessive oxidative damage, heme is actively taken

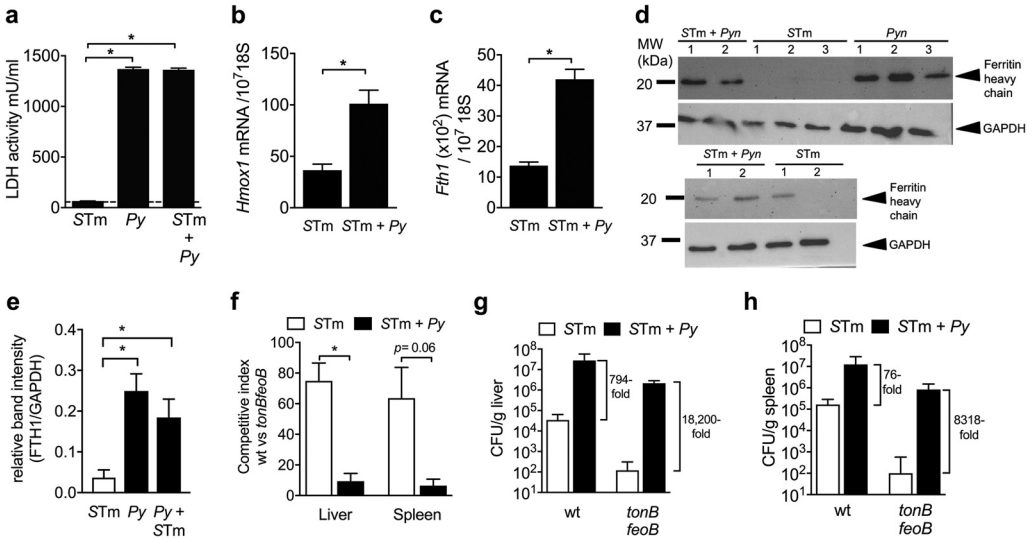

FIG 3 (a) Levels of serum lactate dehydrogenase (LDH) from uninfected, *S.* Typhimurium-infected, *P. yoelii*-infected, and coinfected mice ($n = 3$). Data represent the mean ± SEM. The dashed line represents the average LDH levels from uninfected mice. (b, c) Expression of heme oxygenase-1 (*Hmox1*) (b) and ferritin heavy chain (*Fth1*) (c) from CD11b$^+$ liver cells isolated from *S.* Typhimurium-infected and coinfected mice 2 days after *S.* Typhimurium infection ($n = 3$ to 4). Data represent the mean ± SEM. (d) Western blots showing the abundance of the ferritin heavy chain in CD11b$^+$ liver cells isolated from *S.* Typhimurium-infected, *P. yoelii*-infected, and coinfected mice ($n = 3$ to 5). Data are pooled from two independent experiments. MW, molecular weight. (e) Densitometric quantification of the FTH1 band intensity relative to the GAPDH band intensity on the Western blots from panel d. (f) Competitive index of CFU in the liver and spleen 2 days after i.p. infection of *P. yoelii*-infected or uninfected CBA/J mice with a 1:1 mixture of wild-type (wt) *S.* Typhimurium and the isogenic *tonB feoB* mutant ($n = 3$ to 4). (g, h) Numbers of CFU in the liver (g) and spleen (h) 3 days after i.p. inoculation with either the *S.* Typhimurium wild type or the *tonB feoB* mutant in *P. yoelii*-infected or uninfected CBA/J mice ($n = 4$). Data represent the mean ± SEM. Statistical significance was determined using an unpaired Student *t* test on log-transformed values. *, $P < 0.05$. See also Fig. S3 in the supplemental material.

up by macrophages and detoxified via heme oxygenase-1. We observed a significant increase in the expression of *Hmox1*, encoding heme oxygenase-1, in CD11b$^+$ liver macrophages from coinfected mice compared to *S.* Typhimurium-infected mice (Fig. 3b). During the degradation of heme, iron is released and transported to the cytosol, where it is incorporated into ferritin molecules. In accordance with the increased expression of *Hmox1*, we also observed a significant increase in the expression of ferritin heavy chain 1 (*Fth1*) in CD11b$^+$ liver macrophages isolated from coinfected mice compared to those isolated from *S.* Typhimurium-infected mice (Fig. 3c). Further, the protein levels of ferritin H were increased in CD11b$^+$ liver macrophages isolated from *P. yoelii*-infected and coinfected mice compared to those isolated from *S.* Typhimurium-infected mice (Fig. 3d and e). Interestingly, the increased availability of iron-laden ferritin has been shown to enhance the survival of *S.* Typhimurium in mouse macrophages *in vitro* (9). Furthermore, induction of heme oxygenase-1 in mouse macrophages *in vitro* was associated with an increased iron content and augmented intracellular bacterial replication (11). Taken together, these results suggest that increased iron availability via induction of heme oxygenase-1 might benefit the systemic growth of *S.* Typhimurium during malaria.

In order to test whether *S.* Typhimurium benefits from the increased availability of iron during concurrent *P. yoelii* infection, we performed a competitive infection experiment in which wild-type *S.* Typhimurium was coadministered via the i.p. route with an *S.* Typhimurium *tonB feoB* mutant that was deficient for both ferric and ferrous iron uptake. We found that iron acquisition enhanced the growth of *S.* Typhimurium at systemic sites, because the wild-type strain outcompeted the *tonB feoB* mutant by 120-fold in the liver ($P = 0.02$) and by 102-fold in the spleen ($P = 0.06$) (Fig. 3f). However, the fitness advantage conferred by iron uptake was significantly reduced in the liver and spleen of coinfected mice. Similarly, in mice inoculated individually with

either wild-type *S.* Typhimurium or the *tonB feoB* mutant, the mutant defective for high-affinity iron uptake was rescued by malaria parasite infection to a greater extent than the wild type, suggesting that the underlying *P. yoelii* infection compensated for this deficit (Fig. 3g and h). Taken together, these results suggest that increased iron availability during malaria contributes to the systemic outgrowth of *S.* Typhimurium.

DISCUSSION

While it has been proposed that the redistribution of iron to macrophages during malaria may be a factor predisposing individuals to bacterial superinfection (29), our results provide the first *in vivo* evidence that *S.* Typhimurium benefits from increased iron availability during malaria parasite infection. Increased expression of *Hmox1* in phagocytic cells was associated with enhanced expression of *Fth1*, as well as increased protein levels of the heavy chain of ferritin. Increased ferritin levels suggested that the iron content within macrophages becomes elevated during malaria. As a result, underlying *P. yoelii* infection was sufficient to rescue the growth of an *S.* Typhimurium mutant deficient for high-affinity iron uptake systems. It is known that changes in macrophage iron metabolism can influence macrophage polarization (reviewed in reference 30) and that iron overloading in macrophages *in vitro* is associated with decreased inflammatory activation (31, 32). In the context of malaria, it has been reported that the uptake of *P. falciparum*-infected red blood cells by macrophages induces the production of IL-10, which in turn upregulates hepcidin, leading to the increased intracellular retention of iron (33). Hence, in addition to providing an essential nutrient that enhances bacterial growth, iron overloading could impair the bactericidal activity of macrophages against nontyphoidal *Salmonella*. It has been previously observed that *S.* Typhimurium preferentially associates with macrophages of an anti-inflammatory (M2) phenotype during chronic infection in mice (34–36). During experimental coinfection, we found that liver macrophages were significantly impaired in their ability to induce transcripts encoding key proinflammatory mediators, TNF-α, iNOS, and GM-CSF, and infiltrating monocytes expressed significantly smaller amounts of the inflammatory marker Ly6C, suggestive of an M2 phenotype. Furthermore, the lack of GM-CSF induction in response to *S.* Typhimurium infection during underlying malaria likely contributed to the decreased activation state of liver macrophages. Interestingly, this shift in macrophage activation correlated with the partial rescue of a mutant defective for the T3SS-2 apparatus for systemic replication. Taken together with the findings of Grant and colleagues, who showed that a T3SS-2 mutant is defective for cell-to-cell spread in tissue (13), these results suggest that the phagocytic functions impaired by malaria may be the same ones that T3SS-2 overcomes during systemic infection.

However, it remains unclear what parasite-mediated responses promoted this increase in susceptibility to systemic *S.* Typhimurium infection. We previously observed an increase in circulating IL-10 levels during *P. yoelii* infection (12), and it is known that IL-10 can drive the polarization of macrophages to an anti-inflammatory state. In this study, we showed that the loss of inflammatory monocyte recruitment to the liver during coinfection was partially mediated by parasite induction of IL-10. We have previously shown that the increased production of IL-10 acts on myeloid cells to increase the systemic bacterial loads of *S.* Typhimurium (12). Together these results suggest that the parasite-mediated induction of IL-10 modulates inflammatory cell recruitment and the bactericidal capacity of macrophages, thereby increasing susceptibility to invasive NTS infection. Therefore, further exploration of IL-10 signaling in macrophages and its effect on macrophage activation during malaria parasite and *S.* Typhimurium coinfection is needed.

Taken together with previous reports, our findings suggest that IL-10, in concert with parasite-mediated induction of anemia, may drive the polarization of macrophages to a less inflammatory state, thereby predisposing individuals to invasive NTS infection. Some findings from clinical cases of malaria corroborate this idea: the uptake of *P. falciparum*-parasitized RBCs by human peripheral blood mononuclear cells upregulates their expression of hepcidin, which drives intracellular iron retention (37). In

the liver of fatal malaria cases, high levels of heme oxygenase-1 were detected in Kupffer cells and circulating monocytes (38). Further, children presenting with acute *P. falciparum* malaria had elevated levels of circulating IL-10 (39). Therefore, infection with *S.* Typhimurium during the acute stage of malaria may facilitate initial bacterial colonization and enhance intracellular growth by reducing the proportion of inflammatory macrophages and increasing the proportion of anti-inflammatory macrophages. Taken together, our results suggest that increased levels of heme and the consequent induction of heme oxygenase-1 in macrophages during malaria facilitate invasive NTS infection by modulating host immune responses in combination with increasing the available iron for bacterial growth.

MATERIALS AND METHODS

Ethics statement. Experiments with mice were carried out in strict accordance with the recommendations in the *Guide for the Care and Use of Laboratory Animals* of the National Research Council (40) and were approved by the Institutional Animal Care and Use Committees at the University of California Davis (UC Davis) under protocol 18183.

Mouse strains. Specific-pathogen-free 6- to 8 week-old female CBA/J mice were purchased from The Jackson Laboratory (Bar Harbor, ME). Additionally, C57BL/6J *Slc11a1*$^{+/+}$ and C57BL/6J *Slc11a1*$^{+/+}$ *Il10*$^{-/-}$ mice were bred and maintained by the UC Davis Teaching and Research Animal Care Service. The mice were maintained under specific-pathogen-free conditions by the UC Davis Center for Laboratory Animal Science, receiving irradiated rodent chow and sterile drinking water *ad libitum*. The UC Davis Institutional Animal Care and Use Committee approved all animal experiments described in this report.

***Plasmodium yoelii nigeriensis* (*P. yoelii*).** Parasite stocks were obtained from the Malaria Research and Reference Reagent Resource, and the species was confirmed by DNA sequencing of merozoite surface protein-1 (MSP-1) (41). Parasite stocks were made by passage in CD-1 mice. For coinfection experiments in CBA/J and C57BL/6 mice were inoculated intraperitoneally (i.p.) on day 0 with approximately 4×10^7 or 4×10^6 infected red blood cells (iRBCs), respectively, in 0.1 ml of saline. Mock-infected controls were injected i.p. with an equivalent amount of blood from uninfected CD-1 mice.

***Salmonella enterica* serotype Typhimurium.** The *S.* Typhimurium IR715(pHP45Ω), *S.* Typhimurium *spiB*(pHP45Ω) (a T3SS-2 mutant), and *S.* Typhimurium *tonB feoB* (an iron uptake mutant) strains were used for this study. To ensure consistent infection of resistant CBA/J mice with *S.* Typhimurium, intragastrically (IG) inoculated mice received 20 mg of streptomycin (Sigma) by gavage 24 h prior to infection. Mice received either 0.1 ml of sterile Luria-Bertani (LB) broth, 1×10^8 CFU of *S.* Typhimurium, or 1×10^9 CFU of the *S.* Typhimurium *spiB* mutant in 0.1 ml of LB broth by gastric gavage. Inocula were cultured for 16 h aerobically with selective pressure at 37°C. For i.p. inoculation of *S.* Typhimurium *spiB*, CBA/J mice received 5×10^2 *S.* Typhimurium bacteria in phosphate-buffered saline (PBS) or an equivalent volume of PBS. For i.p. inoculation of single *S.* Typhimurium and *S.* Typhimurium *tonB feoB* mutant infections, CBA/J mice received 1×10^3 CFU of either strain in PBS. For i.p. inoculation of competitive infections, CBA/J mice were i.p. infected with a 1:1 mixture of the *S.* Typhimurium wild type and *S.* Typhimurium *tonB feoB* mutant in a total inoculum of 1×10^4 CFU. For i.p. inoculation of *S.* Typhimurium, wild-type and *Il10*$^{-/-}$ C57BL/6 mice received 1×10^3 CFU of *S.* Typhimurium in PBS or an equivalent volume of PBS.

Microbial readouts of infection. To determine the numbers of viable *Salmonella* bacteria, livers were homogenized in PBS using an Ultra Turrax T25 basic mixer (IKA). Blood was collected from the heart with heparinized needles, and the plasma was removed and then incubated for 10 min with 120 μl 1% Triton X-100 in PBS. Homogenates were serially diluted and plated on LB agar plates containing 100 mg/liter nalidixic acid (Sigma) or 100 mg/liter kanamycin (Sigma). After overnight growth at 37°C, the number of CFU per gram of tissue was calculated.

Flow cytometry. Flow cytometry analysis was performed for the detection of inflammatory monocytes and macrophages in livers from *S.* Typhimurium-infected and coinfected CBA/J mice 4 days after IG bacterial infection. Flow cytometry analysis for detection of inflammatory monocytes in the livers from uninfected, *P. yoelii*-infected, and coinfected C57BL/6J *Slc11a1*$^{+/+}$ and C57BL/6J *Slc11a1*$^{+/+}$ *Il10* mice was performed 2 days after i.p. bacterial infection. Single-cell suspensions of liver tissue were obtained according to the protocol described by Miltenyi Biotec for the preparation of single-cell suspensions from mouse liver. Briefly, livers were perfused with 10 ml of PBS (Gibco) by cardiac puncture, gallbladders were removed aseptically, and the livers were digested with collagenase type IV for 30 min at 37°C. Tissue was dissociated using a gentleMACS dissociator (Miltenyi Biotec) and passed through a 70-μm-pore-size filter. Hepatocytes were removed by centrifugation, and red blood cells were lysed using ACK buffer (Lonza). Liver cells were resuspended in PBS and counted. A total of 4×10^6 cells/mouse were resuspended in 2 ml of PBS and stained with Aqua Live/Dead cell discriminator (Invitrogen) according to the manufacturer's protocol. After Live/Dead staining, the cells were washed with PBS and resuspended in 50 μl of PBS containing 1% bovine serum albumin and 2 mM EDTA (fluorescence-activated cell sorter [FACS] buffer). The cells were stained with an Fc receptor-blocking antibody, anti-CD16/CD32 (eBioscience), for 5 min at 4°C and then stained with a cocktail of anti-B220 phycoerythrin (PE) (BD Biosciences), anti-CD3 PE (BD Biosciences), anti-NK1.1 PE (BioLegend), anti-CD11b PE-Cy7 (eBioscience), Ly6C Pacific Blue (BioLegend), and Ly6G peridinin chlorophyll protein (PerCP)-Cy5.5 (BioLegend) for 30 min at 4°C. Cells were washed in FACS buffer, fixed with 4% paraformaldehyde for 30 min at 4°C, and then resuspended in FACS buffer. Fifty microliters of Sphero AccuCount fluorescent particles (diameter, 10.1 μm; Sphero-

tech) were added to each sample prior to analysis in order to determine absolute counts. Calculation of absolute counts was performed according to the manufacturer's protocol. For experiments that included staining of CD68, cells were first stained with an Fc receptor-blocking antibody, anti-CD16/CD32 (eBioscience), for 5 min at 4°C and then stained with a cocktail of anti-B220 PE (BD Biosciences), anti-CD3 PE (BD Biosciences), anti-NK1.1 PE (BioLegend), anti-CD11b allophycocyanin (APC)-Cy7 (eBioscience), anti-Ly6C Pacific Blue or BV421 (BioLegend), and anti-Ly6G PerCP-Cy5.5 (BioLegend) for 30 min at 4°C. Cells were washed in FACS buffer, fixed, and permeabilized with BD Cytofix/Cytoperm solution (BD Biosciences) for 20 min at 4°C and then washed twice with BD Perm/Wash buffer (BD Biosciences). Cells were resuspended in 100 μl of BD Perm/Wash buffer containing anti-CD68 APC (BioLegend) and incubated in the dark at 4°C for 30 min. Cells were washed in BD Perm/Wash buffer and resuspended in FACS buffer. Flow cytometry analysis was performed using an LSRII apparatus (Becton Dickinson), and 7.5×10^5 events were collected per mouse. The resulting data were analyzed using FlowJo software (TreeStar, Inc., Ashland, OR). Gates were based on fluorescence-minus-one (FMO) controls.

Liver CD11b$^+$ macrophage isolation. Liver single-cell suspensions were isolated as described above. In order to separate out granulocytes, liver single-cell suspensions were diluted in 3 ml of Dulbecco's PBS (dPBS), layered on top of 3 ml of Ficoll-Paque Plus, and centrifuged at 400 $\times$ *g* for 40 min at 25°C without the brake. The upper layer, which included mononuclear cells, was drawn off and washed twice with dPBS. Cells were resuspended in dPBS containing 2% fetal bovine serum and 1 mM EDTA. Isolation of CD11b$^+$ cells was performed using an EasySepMouse CD11b positive selection kit II (Stemcell Technologies) according to the manufacturer's protocol.

RNA extraction, RT-PCR, and real-time PCR. RNA isolation from purified CD11b$^+$ liver cells was performed on the same day. RNA was extracted from samples using the Tri-Reagent (Molecular Research Center, Cincinnati, OH, USA) according to the manufacturer's instructions. All RNA samples were treated with DNase I (Ambion, Austin, TX, USA) to remove genomic DNA contamination. For quantification of mRNA levels, 0.4 μg of total RNA from each sample was reverse transcribed in a 50-μl volume (TaqMan reverse transcription [RT] reagent; Applied Biosystems, Foster City, CA, USA), and 4 μl of cDNA was used for each real-time reaction. Real-time PCR was performed using the primers listed in Table S1 in the supplemental material, SYBR green (Applied Biosystems), and a ViiA 7 real-time PCR system (Applied Biosystems). Target gene transcription of each sample was normalized to the respective levels of 18S rRNA, and absolute quantification was determined using gene-specific plasmid standards in each run.

M-CSF and GM-CSF ELISAs. Serum M-CSF and GM-CSF from uninfected, *S.* Typhimurium-infected, *P. yoelii*-infected, and coinfected mice were quantified by enzyme-linked immunosorbent assay (ELISA; R&D Systems, Minneapolis, MN, USA), according to the manufacturer's instructions. The ELISA was read at 450 nm with an ELISA microplate reader (model 680; Bio-Rad, Hercules, CA, USA). Data points are the averages for duplicate dilutions.

Serum LDH measurement. Blood was collected from the heart with heparinized needles at necropsy and centrifuged at 8,000 rpm for 5 min. Plasma was removed and stored at −80°C. A lactate dehydrogenase (LDH) colorimetric assay kit (Abcam) was used to quantify the levels of LDH.

Western blotting. Protein was extracted from CD11b$^+$ liver cells using the Tri-Reagent (Molecular Research Center, Cincinnati, OH, USA) according to the manufacturer's instructions. Protein was separated by SDS-PAGE and transferred to a polyvinylidene fluoride membrane (Millipore). A blocking solution of 2.5% nonfat dried milk and 0.1% Tween 20 (Bio-Rad) in PBS was used. For ferritin heavy chain detection, a 1:1,000 dilution of the primary antibody (anti-ferritin heavy chain rabbit monoclonal antibody [MAb]; Abcam) in blocking solution was added to the membrane. As a loading control, GADPH (glyceraldehyde-3-phosphate dehydrogenase) was detected at a 1:5,000 dilution of the primary antibody (GAPDH rabbit MAb; Cell Signaling) in blocking solution. A donkey anti-rabbit immunoglobulin horseradish peroxidase (HRP)-conjugated secondary antibody (Bio-Rad) was diluted 1:3,000 in blocking buffer and applied to the membrane. Protein bands were visualized by chemiluminescence (SuperSignal West Femto maximum sensitivity substrate; Thermo Fisher Scientific) using a BioSpectrum (UVP) imaging system. Raw images were processed using Photoshop CS2 software (Adobe Systems) to uniformly adjust the brightness.

To quantify Western blot images, band intensities were estimated by capturing the area density using LabWorks image acquisition and analysis software (version 4.6.00.0). The gray-level total density of each FTH1 band was normalized to that of the GAPDH band for each sample and displayed as a ratio of relative band intensities. Quantified Western blotting data are shown as mean $\pm$ standard error of the mean (SEM) values for 3 to 5 animals total from two experiments. The statistical significance of the differences between groups was determined by a one-way analysis of variance on log-transformed data, followed by the Sidak multiple-comparison test. A *P* value of 0.05 or less was considered significant.

Statistical analysis. The statistical significance of differences between groups was determined by Student's *t* test on logarithmically or arc-sin-transformed data. A *P* value of 0.05 or less was considered significant. All data were analyzed using two-tailed tests.

SUPPLEMENTAL MATERIAL

Supplemental material for this article may be found at https://doi.org/10.1128/IAI.00301-18.

SUPPLEMENTAL FILE 1, PDF file, 0.9 MB.

ACKNOWLEDGMENTS

This work was supported by USPHS grants AI098078 and AI126860. K.L.L. was supported by American Heart Association predoctoral fellowship 15PRE21420011 and USPHS grant T32AI060555. A.R.S.-L. was supported by USPHS grant UL1 TR001860 and linked award TL1 TR001861. Flow cytometry was performed in a facility supported by facilities improvement grant RR12088-01.

REFERENCES

1. Sanchez-Vargas FM, Abu-El-Haija MA, Gomez-Duarte OG. 2011. Salmonella infections: an update on epidemiology, management, and prevention. Travel Med Infect Dis 9:263–277. https://doi.org/10.1016/j.tmaid.2011.11.001.
2. Feasey NA, Dougan G, Kingsley RA, Heyderman RS, Gordon MA. 2012. Invasive non-typhoidal salmonella disease: an emerging and neglected tropical disease in Africa. Lancet 379:2489–2499. https://doi.org/10.1016/S0140-6736(11)61752-2.
3. Bronzan RN, Taylor TE, Mwenechanya J, Tembo M, Kayira K, Bwanaisa L, Njobvu A, Kondowe W, Chalira C, Walsh AL, Phiri A, Wilson LK, Molyneux ME, Graham SM. 2007. Bacteremia in Malawian children with severe malaria: prevalence, etiology, HIV coinfection, and outcome. J Infect Dis 195:895–904. https://doi.org/10.1086/511437.
4. Nielsen MV, Sarpong N, Krumkamp R, Dekker D, Loag W, Amemasor S, Agyekum A, Marks F, Huenger F, Krefis AC, Hagen RM, Adu-Sarkodie Y, May J, Schwarz NG. 2012. Incidence and characteristics of bacteremia among children in rural Ghana. PLoS One 7:e44063. https://doi.org/10.1371/journal.pone.0044063.
5. Oundo JO, Muli F, Kariuki S, Waiyaki PG, Iijima Y, Berkley J, Kokwaro GO, Ngetsa CJ, Mwarumba S, Torto R, Lowe B. 2002. Non-typhi salmonella in children with severe malaria. East Afr Med J 79:633–639. https://doi.org/10.4314/eamj.v79i12.8670.
6. Gordon MA. 2011. Invasive nontyphoidal Salmonella disease: epidemiology, pathogenesis and diagnosis. Curr Opin Infect Dis 24:484–489. https://doi.org/10.1097/QCO.0b013e32834a9980.
7. Perkins DJ, Were T, Davenport GC, Kempaiah P, Hittner JB, Ong'echa JM. 2011. Severe malarial anemia: innate immunity and pathogenesis. Int J Biol Sci 7:1427–1442. https://doi.org/10.7150/ijbs.7.1427.
8. Choi AM, Alam J. 1996. Heme oxygenase-1: function, regulation, and implication of a novel stress-inducible protein in oxidant-induced lung injury. Am J Respir Cell Mol Biol 15:9–19. https://doi.org/10.1165/ajrcmb.15.1.8679227.
9. Nairz M, Theurl I, Ludwiczek S, Theurl M, Mair SM, Fritsche G, Weiss G. 2007. The co-ordinated regulation of iron homeostasis in murine macrophages limits the availability of iron for intracellular Salmonella typhimurium. Cell Microbiol 9:2126–2140. https://doi.org/10.1111/j.1462-5822.2007.00942.x.
10. Cunnington AJ, de Souza JB, Walther M, Riley EM. 2011. Malaria impairs resistance to Salmonella through heme- and heme oxygenase-dependent dysfunctional granulocyte mobilization. Nat Med 18:120–127. https://doi.org/10.1038/nm.2601.
11. Mitterstiller AM, Haschka D, Dichtl S, Nairz M, Demetz E, Talasz H, Soares MP, Einwallner E, Esterbauer H, Fang FC, Geley S, Weiss G. 2016. Heme oxygenase 1 controls early innate immune response of macrophages to Salmonella Typhimurium infection. Cell Microbiol 18:1374–1389. https://doi.org/10.1111/cmi.12578.
12. Lokken KL, Mooney JP, Butler BP, Xavier MN, Chau JY, Schaltenberg N, Begum RH, Muller W, Luckhart S, Tsolis RM. 2014. Malaria parasite infection compromises control of concurrent systemic non-typhoidal Salmonella infection via IL-10-mediated alteration of myeloid cell function. PLoS Pathog 10:e1004049. https://doi.org/10.1371/journal.ppat.1004049.
13. Grant AJ, Morgan FJ, McKinley TJ, Foster GL, Maskell DJ, Mastroeni P. 2012. Attenuated Salmonella Typhimurium lacking the pathogenicity island-2 type 3 secretion system grow to high bacterial numbers inside phagocytes in mice. PLoS Pathog 8:e1003070. https://doi.org/10.1371/journal.ppat.1003070.
14. Richter-Dahlfors A, Buchan AM, Finlay BB. 1997. Murine salmonellosis studied by confocal microscopy: Salmonella typhimurium resides intracellularly inside macrophages and exerts a cytotoxic effect on phagocytes in vivo. J Exp Med 186:569–580. https://doi.org/10.1084/jem.186.4.569.
15. Salcedo SP, Noursadeghi M, Cohen J, Holden DW. 2001. Intracellular replication of Salmonella typhimurium strains in specific subsets of splenic macrophages in vivo. Cell Microbiol 3:587–597. https://doi.org/10.1046/j.1462-5822.2001.00137.x.
16. Nakoneczna I, Hsu HS. 1980. The comparative histopathology of primary and secondary lesions in murine salmonellosis. Br J Exp Pathol 61:76–84.
17. Sunderkotter C, Nikolic T, Dillon MJ, Van Rooijen N, Stehling M, Drevets DA, Leenen PJ. 2004. Subpopulations of mouse blood monocytes differ in maturation stage and inflammatory response. J Immunol 172:4410–4417. https://doi.org/10.4049/jimmunol.172.7.4410.
18. Yang J, Zhang L, Yu C, Yang XF, Wang H. 2014. Monocyte and macrophage differentiation: circulation inflammatory monocyte as biomarker for inflammatory diseases. Biomark Res 2:1. https://doi.org/10.1186/2050-7771-2-1.
19. Lloyd CM, Phillips AR, Cooper GJ, Dunbar PR. 2008. Three-colour fluorescence immunohistochemistry reveals the diversity of cells staining for macrophage markers in murine spleen and liver. J Immunol Methods 334:70–81. https://doi.org/10.1016/j.jim.2008.02.005.
20. Rydstrom A, Wick MJ. 2007. Monocyte recruitment, activation, and function in the gut-associated lymphoid tissue during oral Salmonella infection. J Immunol 178:5789–5801. https://doi.org/10.4049/jimmunol.178.9.5789.
21. Burgess AW, Metcalf D. 1980. The nature and action of granulocyte-macrophage colony stimulating factors. Blood 56:947–958.
22. Hamilton JA. 2008. Colony-stimulating factors in inflammation and autoimmunity. Nat Rev Immunol 8:533–544. https://doi.org/10.1038/nri2356.
23. Fleetwood AJ, Lawrence T, Hamilton JA, Cook AD. 2007. Granulocyte-macrophage colony-stimulating factor (CSF) and macrophage CSF-dependent macrophage phenotypes display differences in cytokine profiles and transcription factor activities: implications for CSF blockade in inflammation. J Immunol 178:5245–5252. https://doi.org/10.4049/jimmunol.178.8.5245.
24. Martinez FO, Gordon S, Locati M, Mantovani A. 2006. Transcriptional profiling of the human monocyte-to-macrophage differentiation and polarization: new molecules and patterns of gene expression. J Immunol 177:7303–7311. https://doi.org/10.4049/jimmunol.177.10.7303.
25. Verreck FA, de Boer T, Langenberg DM, Hoeve MA, Kramer M, Vaisberg E, Kastelein R, Kolk A, de Waal-Malefyt R, Ottenhoff TH. 2004. Human IL-23-producing type 1 macrophages promote but IL-10-producing type 2 macrophages subvert immunity to (myco)bacteria. Proc Natl Acad Sci U S A 101:4560–4565. https://doi.org/10.1073/pnas.0400983101.
26. Hamilton JA. 1994. Coordinate and noncoordinate colony stimulating factor formation by human monocytes. J Leukoc Biol 55:355–361. https://doi.org/10.1002/jlb.55.3.355.
27. Lee MT, Kaushansky K, Ralph P, Ladner MB. 1990. Differential expression of M-CSF, G-CSF, and GM-CSF by human monocytes. J Leukoc Biol 47:275–282. https://doi.org/10.1002/jlb.47.3.275.
28. Coon C, Beagley KW, Bao S. 2009. The role of granulocyte macrophage-colony stimulating factor in gastrointestinal immunity to salmonellosis. Scand J Immunol 70:106–115. https://doi.org/10.1111/j.1365-3083.2009.02279.x.
29. Spottiswoode N, Duffy PE, Drakesmith H. 2014. Iron, anemia and hepcidin in malaria. Front Pharmacol 5:125. https://doi.org/10.3389/fphar.2014.00125.
30. Nairz M, Schroll A, Demetz E, Tancevski I, Theurl I, Weiss G. 2015. 'Ride on the ferrous wheel'—the cycle of iron in macrophages in health and disease. Immunobiology 220:280–294. https://doi.org/10.1016/j.imbio.2014.09.010.
31. Nairz M, Schleicher U, Schroll A, Sonnweber T, Theurl I, Ludwiczek S, Talasz H, Brandacher G, Moser PL, Muckenthaler MU, Fang FC, Bogdan C, Weiss G. 2013. Nitric oxide-mediated regulation of ferroportin-1 controls

macrophage iron homeostasis and immune function in Salmonella infection. J Exp Med 210:855–873. https://doi.org/10.1084/jem.20121946.
32. Gan ZS, Wang QQ, Li JH, Wang XL, Wang YZ, Du HH. 2017. Iron reduces M1 macrophage polarization in RAW264.7 macrophages associated with inhibition of STAT1. Mediators Inflamm 2017:8570818. https://doi.org/10.1155/2017/8570818.
33. Huang H, Lamikanra AA, Alkaitis MS, Thezenas ML, Ramaprasad A, Moussa E, Roberts DJ, Casals-Pascual C. 2014. Interleukin-10 regulates hepcidin in Plasmodium falciparum malaria. PLoS One 9:e88408. https://doi.org/10.1371/journal.pone.0088408.
34. Eisele NA, Ruby T, Jacobson A, Manzanillo PS, Cox JS, Lam L, Mukundan L, Chawla A, Monack DM. 2013. Salmonella require the fatty acid regulator PPARdelta for the establishment of a metabolic environment essential for long-term persistence. Cell Host Microbe 14:171–182. https://doi.org/10.1016/j.chom.2013.07.010.
35. Nix RN, Altschuler SE, Henson PM, Detweiler CS. 2007. Hemophagocytic macrophages harbor Salmonella enterica during persistent infection. PLoS Pathog 3:e193. https://doi.org/10.1371/journal.ppat.0030193.
36. McCoy MW, Moreland SM, Detweiler CS. 2012. Hemophagocytic macrophages in murine typhoid fever have an anti-inflammatory phenotype. Infect Immun 80:3642–3649. https://doi.org/10.1128/IAI.00656-12.
37. Armitage AE, Pinches R, Eddowes LA, Newbold CI, Drakesmith H. 2009. Plasmodium falciparum infected erythrocytes induce hepcidin (HAMP) mRNA synthesis by peripheral blood mononuclear cells. Br J Haematol 147:769–771. https://doi.org/10.1111/j.1365-2141.2009.07880.x.
38. Clark IA, Awburn MM, Harper CG, Liomba NG, Molyneux ME. 2003. Induction of HO-1 in tissue macrophages and monocytes in fatal falciparum malaria and sepsis. Malar J 2:41. https://doi.org/10.1186/1475-2875-2-41.
39. Mandala WL, Msefula CL, Gondwe EN, Drayson MT, Molyneux ME, MacLennan CA. 2017. Cytokine profiles in Malawian children presenting with uncomplicated malaria, severe malarial anemia, and cerebral malaria. Clin Vaccine Immunol 24:e00533-16. https://doi.org/10.1128/CVI.00533-16.
40. National Research Council. 2011. Guide for the care and use of laboratory animals, 8th ed. National Academies Press, Washington, DC.
41. Roux CM, Butler BP, Chau JY, Paixao TA, Cheung KW, Santos RL, Luckhart S, Tsolis RM. 2010. Both hemolytic anemia and malaria parasite-specific factors increase susceptibility to nontyphoidal Salmonella enterica serovar Typhimurium infection in mice. Infect Immun 78:1520–1527. https://doi.org/10.1128/IAI.00887-09.